


Article

An Analytical Solution for Block Toppling Failure of Rock Slopes during an Earthquake

Songfeng Guo ^{1,2}, Shengwen Qi ^{1,2,*}, Guoxiang Yang ³, Shishu Zhang ⁴ and Charalampos Saroglou ⁵ 

¹ Key Laboratory of Shale Gas and Geoenvironment, Institute of Geology and Geophysics, Chinese Academy of Sciences, Beijing 100029, China; guosongfeng@mail.iggcas.ac.cn

² College of Earth Science, University of Chinese Academy of Sciences, Beijing 100049, China

³ School of Engineering and Technology, China University of Geosciences (Beijing), Beijing 100083, China; yanggx@cugb.edu.cn

⁴ Chengdu Engineering Corporation Limited, Power China, Chengdu 610072, China; geochidi@163.com

⁵ School of Civil Engineering, National Technical University of Athens, Athens 15773, Greece; saroglou@central.ntua.gr

* Correspondence: qishengwen@mail.iggcas.ac.cn

Received: 7 August 2017; Accepted: 20 September 2017; Published: 29 September 2017

Featured Application: Rock slope stability under earthquake.

Abstract: Toppling failure is one of the most common failure types in the field. It always occurs in rock masses containing a group of dominant discontinuities dipping into the slope. Post-earthquake investigation has shown that many toppling rock slope failures have occurred during earthquakes. In this study, an analytical solution is presented on the basis of limit equilibrium analysis. The acceleration of seismic load as well as joint persistence within the block base, were considered in the analysis. The method was then applied into a shake table test of an anti-dip layered slope model. As predicted from the analytical method, blocks topple or slide from slope crest to toe progressively and the factor of safety decreases as the inputting acceleration increases. The results perfectly duplicate the deformation features and stability condition of the physical model under the shake table test. It is shown that the presented method is more universal than the original one and can be adopted to evaluate the stability of the slope with potential toppling failure under seismic loads.

Keywords: earthquake; block toppling; analytical solution; slope stability; limit equilibrium method

1. Introduction

Toppling failures always occur in rock masses with a dominant discontinuity set (usually bedding or foliation) which strike parallel to the slope and dip inwards. This failure mode is one of the most common seen in natural or excavated rock slopes, e.g., rock slopes induced by construction including of hydropower stations [1–3], open-pit mines [4,5], railway [5] and other engineering works [6]. In recent years, quite a number of toppling failures occurred during earthquakes and caused huge losses to lives as well as infrastructures. For example, Xiaojianping landslide and Guantan landslide [7] were both triggered by the Wenchuan earthquake and characterized by an anti-dipping structure (Figure 1). This type of event always occurs abruptly and results in catastrophic loss, e.g., a dammed lake with deposits of about 6,000,000 m³ caused by Xiaojianping landslide.

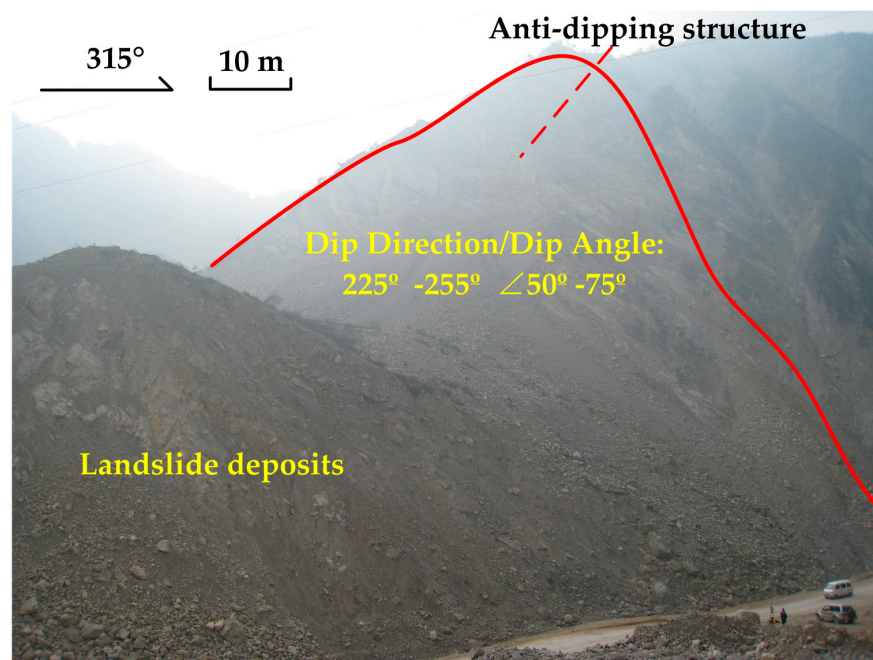


Figure 1. Xiaojianping landslide induced by Wenchuan earthquake on 12 May 2008.

Toppling failure of rock slopes can be roughly differentiated into three modes: block toppling, flexural toppling and combined block and flexural toppling [8]. Numerical approaches, physical models and theoretical analysis are three main tools to study the toppling rock slopes. This study concentrates on the theoretical analysis on the basis of limit equilibrium method. The quantitative limit equilibrium method to evaluate the stability of block toppling rock slopes was originally proposed by [8], after which this method has been largely further developed. Zank (1983) [9] gave a design chart for rock slopes susceptible to toppling based on the original analytical solution. Bobet (1999) [10] presented an analytical method for the toppling failure considering the toppling mass as continuous medium rather than a discrete assemblage of blocks. Sagaseta et al. (2001) [11] derived an analytical solution also considering the infinitesimal thickness of blocks and concluded that this method is suitable for slopes higher than 20–30 times the average block thickness. Chen et al. (2005) [1] made an extension of the original solution considering the connectivity of block base. Liu et al. (2008, 2010) [12,13] extended the continuum solution developed by [10,11] and presented an analytical approach for analyzing block toppling of those slopes that can be considered as continua. Considering rock layers as cantilever beams, Aydan and Kawamoto (1992) [14] proposed a limit equilibrium stability analysis method for slopes and underground openings under various loading conditions against the flexural toppling. Adihikary et al. (1997) [15] adopted this limit equilibrium approach to analyze a centrifuge test data and found this method can accurately predict the failure load for the tests. Majdi and Amini (2011) [16] conducted studies on flexural toppling considering the length of cracks. They presented an equation for length of critical crack, and stated that if the length of natural crack is smaller than that of critical crack, the solid mechanics should be adopted, while otherwise, the fracture mechanics are more suitable. There are few reports about limit equilibrium on the combined block and flexural toppling mode.

It is worth mentioning that seismic loads were taken into account in some new developed analytical solutions in recent years. For example, Yagoda-Biran and Hatzor (2013) [17] presented a 3D failure mode chart for toppling and sliding failure of slope, in which the seismic load is considered as a pseudo-static horizontal force acting at the centroid. However, just one block is considered in this analysis. Zheng et al. (2014) [18] proposed a solution for toppling failure of rock slopes subjected to earthquake, with the slenderness ratio of the block over 20. However, the joint persistence of the

block base is not considered in their solution. Maiorano et al. (2015) [19] investigated the rocking and overturning response of slender rock blocks on a stiff base submitted to simple cyclic excitations and to natural earthquakes. Their study neglects interaction forces within blocks and each block is assumed to be completely detached from the cliff and located on a horizontal plane, meanwhile the sliding failure is excluded by setting a very large friction coefficient at the base of the block. Zhang et al. (2016) [20] conducted research on the rock toppling failure mode subjected to earthquake based on numerical modelling. ROCSCIENCE INC. (2014) [21] presented a 2D limit equilibrium program named RocTopple to perform toppling analysis based on the block toppling method of [8]. RocTopple can display the potential failure mode of individual blocks as well as the overall safety factor with the inputting slope parameters, discontinuity spacing dip angle and strength. The external loads can be applied including seismic load, water pressure, etc. The program provides a convenient way to assess the stability and failure modes of block toppling rock slope subjected to an earthquake. Nevertheless, the amplification effects of seismic acceleration during seismic wave transmitting in the slope and connectivity condition of the joint are excluded in the program.

In this paper, a limit equilibrium solution for block toppling failure during an earthquake is proposed, in which the connectivity of the joint in block base and the interaction force transfer between adjacent blocks are considered. Finally, the solution is adopted to predict the failure modes of individual blocks and the stability of an anti-dip rock slope model under the shake table test.

2. Mechanical Model and Analytical Solution to Toppling Slope Failure

Similar to [1,8,12], the geometry of a toppling slope was simplified as shown in Figure 2. The variables and the corresponding description are addressed in the Abbreviations section at the end of this paper. The mechanical parameters including cohesions, friction angles of joints or bedding planes and tensile strength of blocks can be obtained based on lab or field experiments. Some of the basic geometric parameters can be obtained through field work, such as $\psi_b, \psi_p, \psi_s, \psi_d, \psi_f$ and Δx can be obtained based on field work. The equations to reach other geometric parameters including a_1, a_2, b and y_n can be addressed in Appendix A.

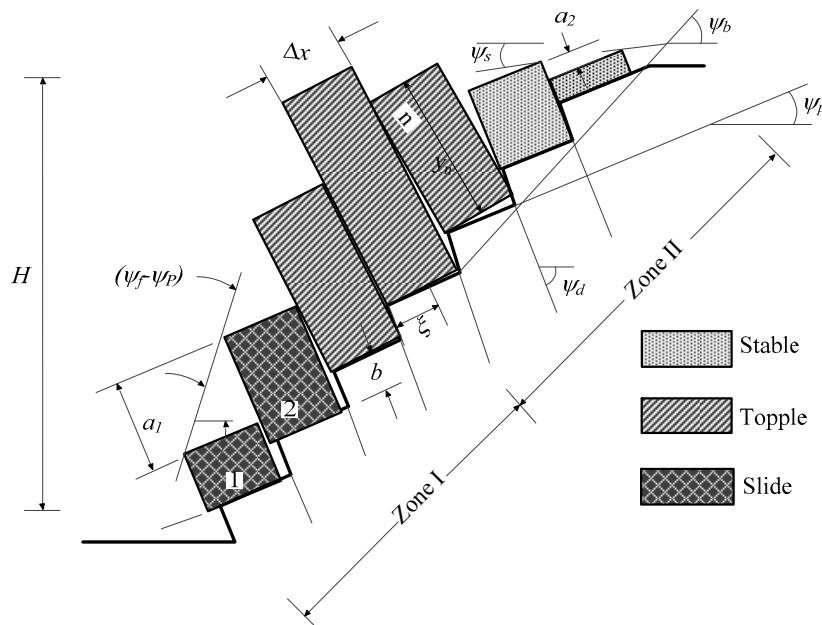


Figure 2. The geometric model of a toppling slope (modified based on [22] after [8]).

It is shown that the interface between deformation blocks and the base is stepped, and its overall dip ψ_b can be valued in the range shown in Equation (1) [8,14,23].

$$\psi_b \approx (\psi_p + 10^\circ) \text{ to } (\psi_p + 30^\circ) \tag{1}$$

The model includes stable and unstable blocks, the latter of which can be divided into toppling blocks and sliding blocks according to the deformation mechanism. The mechanical conditions of the n th toppling block are interpreted in Figure 3. It can be seen that there are normal and shear forces (P_n, Q_n) from the upper block on the right side, (P_{n-1}, Q_{n-1}) from the lower block on the left side, and (R_n, S_n) from the matrix on the base. The approach to reach the geometric parameters M_n, L_n above, at and below the crest is addressed in Appendix A.

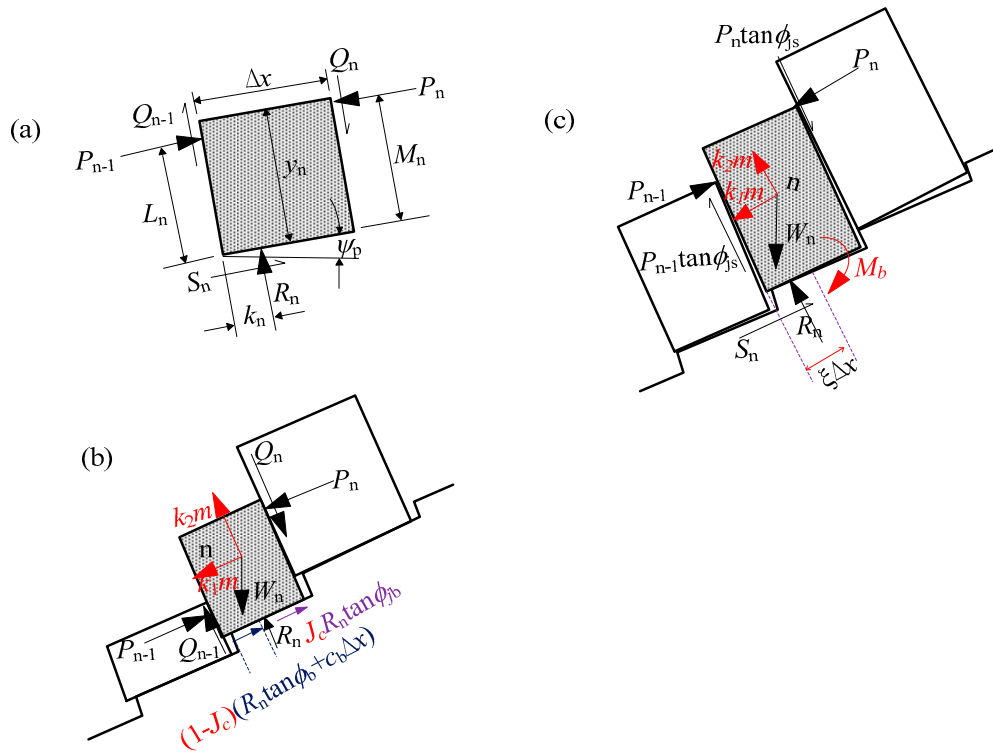


Figure 3. The mechanical condition for the n th block with non-persistent joint on the base under earthquake (modified based on [22] after [8]). (a) External forces from adjacent blocks acting on the n th block; (b) The limit equilibrium condition of the n th toppling block; (c) The limit equilibrium condition of the n th sliding block.

The seismic load acting on the block can be broken down into two components, i.e., k_1 and k_2 . The equilibrium equation for sliding of the n th block can be given as (Figure 3b)

$$R_n = W_n \cos \psi_p + (P_n - P_{n-1}) \tan \phi_{js} - k_2 W_n / g \tag{2}$$

$$\begin{aligned} S_n &= J_c R_n \tan \phi_{jb} + (1 - J_c)(R_n \tan \phi_b + c_b \Delta x) \\ &= W_n \sin \psi_p + (P_n - P_{n-1}) + k_1 W_n / g \end{aligned} \tag{3}$$

So the solution of the force needed from the lower block to keep the n th block from sliding can be obtained as follows:

$$P_{n-1,s} = P_n - \frac{[\sin \psi_p + k_1 / g - (J_c \tan \phi_{jb} + \zeta \tan \phi_b) (\cos \psi_p - k_2 / g)] W_n - \zeta c_b \Delta x}{(J_c \tan \phi_{jb} + \zeta \tan \phi_b) \tan \phi_{js} - 1} \tag{4}$$

The equilibrium equation for toppling of the n th block can be given as (Figure 3c):

$$\begin{aligned}
 &P_{n-1}L_n + W_n(\cos \psi_p - k_2/g)\Delta x/2 + P_n \tan \phi_{js}\Delta x + M_b \\
 &= P_nM_n + W_n(\sin \psi_p + k_1/g)y_n/2 + R_n\epsilon\Delta x/2
 \end{aligned}
 \tag{5}$$

The bases of toppling blocks are acted on with normal forces R_n , shear forces S_n and moment M_b (Figure 3b). It should be noted that the effects of other forces have been incorporated in the three values. The block base can be seen as an eccentric compression bar (Figure 4), so the stress in the base section induced by M_b as

$$\sigma_M = \frac{M_b x}{I_y}
 \tag{6}$$

in which x denotes distance to a neutral point, and I_y denotes the product of inertia of the cross-section to the y axis, $I_y = \frac{1}{12}(\xi\Delta x)^3$, $\xi = 1 - J_c$.

The maximum tensile stress induced by moment M_b occurs at the left edge of the rock bridge on the base (point O in Figure 4):

$$\sigma_{tM} = \frac{M_b \times \frac{1}{2}\xi\Delta x}{\frac{1}{12}(\xi\Delta x)^3} = \frac{M_b}{\frac{1}{6}(\xi\Delta x)^2}
 \tag{7}$$

The compressive stress induced by R_n is uniform on the base:

$$\sigma_{tR} = \frac{R_n}{\xi\Delta x}
 \tag{8}$$

Therefore, the maximum tensile stress occurs at the left edge of the rock bridge on the base:

$$\sigma_t = \frac{M_b}{\frac{1}{6}\xi^2\Delta x^2} - \frac{R_n}{\xi\Delta x}
 \tag{9}$$

So

$$M_b = \frac{\xi\Delta x}{6}(\sigma_t\xi\Delta x + R_n)
 \tag{10}$$

So the solution of the force needed from the lower block to keep the n th block from toppling can be obtained as follows:

$$P_{n-1,t} = \frac{(M_n + \frac{1}{3}\xi\Delta x \tan \phi_{js} - \Delta x \tan \phi_{js})P_n + \frac{\Delta x W_n}{2} \left(1 - \frac{\xi}{6}\right) \left(\frac{k_2}{g} - \cos \psi_p\right) - \frac{\xi^2\Delta x^2}{6}\sigma_t + \frac{v_n W_n}{2} \left(\sin \psi_p + \frac{k_1}{g}\right)}{L_n + \frac{\xi\Delta x}{3} \tan \phi_{js}}
 \tag{11}$$

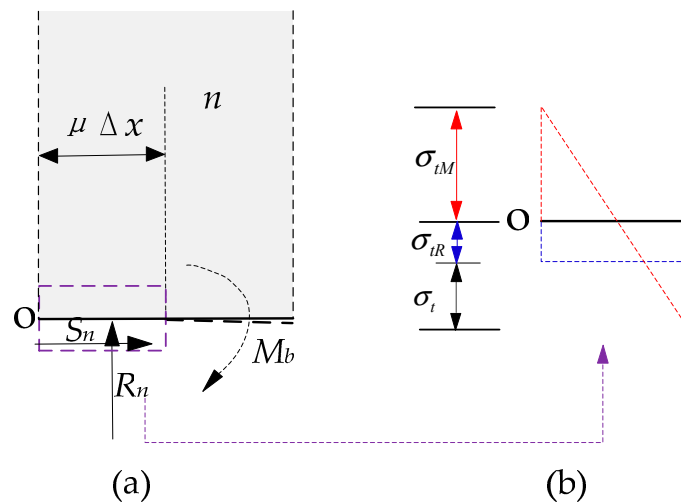


Figure 4. The toppling mechanical condition on the base with non-persistent joint (Modified based on [1]): (a) the mechanical condition of the block base; (b) the stress distribution along the block base.

The dynamic loads as well as joint connectivity rate are taken into account in the limit equilibrium method compared with the original form proposed by [8]. For the special state of static conditions and a persistent block base, the limit equilibrium Equation (4) of sliding and Equation (11) of toppling would be simplified as Equations (12) and (13) respectively. Equations (12) and (13) are the same as the original form proposed by [8]. It can be seen that the proposed solutions are a universal form that can estimate the deformation status and factor of safety (FOS) for toppling slope with various J_c of the block base under different seismic loads.

$$P_{n-1,s} = P_n - \frac{W_n (\cos \psi_p \tan \phi_{jb} - \sin \psi_p)}{1 - \tan \phi_{js} \tan \phi_{jb}} \tag{12}$$

$$P_{n-1,t} = \left[(M_n - \Delta x \tan \phi_{js}) P_n + \frac{W_n}{2} (y_n \sin \psi_p - \Delta x \cos \psi_p) \right] / L_n \tag{13}$$

The solution can be applied by following these steps:

- (1) Reach the basic geometric parameters $\psi_b, \psi_p, \psi_s, \psi_d, \psi_f$ and Δx from in-situ measurement work and calculating other geometric parameters a_1, a_2, b, y_n, M_n and L_n according to Equations (A1)–(A11).
- (2) Determining all the physical parameters of the joints and blocks, e.g., $\rho, \phi_{jb}, \phi_{js}, \phi_b, c_b, \sigma_{bt}$, and the joint connectivity rate (J_c) of the block base on the basis of lab tests, in-situ measurement or experience.
- (3) Calculating $P_{n-1,s}$ and $P_{n-1,t}$ from the top block downwards on the basis of Equations (4) and (11).
- (4) Determining P_{n-1} and the deformation status of the n th block.

If $P_{n-1,s} < 0$ and $P_{n-1,t} < 0, P_{n-1} = 0$. It means that the n th block is stable and does not need the support of the $(n - 1)$ th block.

If $P_{n-1,s} < 0$ and $P_{n-1,t} > 0, P_{n-1} = P_{n-1,t}$. It means that the n th block needs the support of the $(n - 1)$ th block to inhibit toppling deformation.

If $P_{n-1,t} > P_{n-1,s} > 0, P_{n-1} = P_{n-1,t}$. It means that the n th block needs more support from the $(n - 1)$ th block to inhibit toppling failure rather than sliding failure.

If $P_{n-1,s} > 0$ and $P_{n-1,t} < 0, P_{n-1} = P_{n-1,s}$. It means that the n th block needs the support of the $(n - 1)$ th block to inhibit sliding deformation.

If $P_{n-1,s} > P_{n-1,t} > 0, P_{n-1} = P_{n-1,s}$. It means that the n th block needs more support from the $(n - 1)$ th block to inhibit sliding failure rather than toppling failure.

In summary, P_{n-1} can also be simply obtained according to Equation (14):

$$P_{n-1} = \max(P_{n-1,s}, P_{n-1,t}, 0) \tag{14}$$

If $P_{n-1} = 0$, the n th block is stable;

If $P_{n-1} = P_{n-1,t}$, the n th block is toppling;

If $P_{n-1} = P_{n-1,s}$, the n th block is sliding.

P_{n-1} and the deformation status can also be determined according to Table 1.

- (5) Estimating the stability of the slope. If the deformation status of the lowest block ($n = 1$) is stable (or $P_0 = 0$), the slope is stable. If the deformation status of the lowest block ($n = 1$) is unstable (or $P_0 > 0$), the slope is unstable.
- (6) Determining the FOS. The FOS of the slope can be determined using the methods as follows:

A ratio R_q is adopted to obtain the parameters in calculation based on the actual parameters, which are shown as Equations (15)–(19).

$$\tan \phi_{jb}^{calculation} = \tan \phi_{jb}^{actual} / R_a \tag{15}$$

$$\tan \phi_{js}^{calculation} = \tan \phi_{js}^{actual} / R_a \tag{16}$$

$$\tan \phi_b^{calculation} = \tan \phi_b^{actual} / R_a \tag{17}$$

$$c_b^{calculation} = c_b^{actual} / R_a \tag{18}$$

$$\sigma_{bt}^{calculation} = \sigma_{bt}^{actual} / R_a \tag{19}$$

Table 1. Determination of the P_{n-1} and deformation status of the n th block.

Calculating Results			P_{n-1}	Deformation Status
$P_{n-1,t} < 0$	$P_{n-1,s} < 0$	-	0	stable
$P_{n-1,t} > 0$	$P_{n-1,s} < 0$	-	$P_{n-1,t}$	toppling
$P_{n-1,t} > 0$	$P_{n-1,s} > 0$	$P_{n-1,t} > P_{n-1,s}$	$P_{n-1,t}$	toppling
$P_{n-1,t} < 0$	$P_{n-1,s} > 0$	-	$P_{n-1,s}$	sliding
$P_{n-1,t} > 0$	$P_{n-1,s} > 0$	$P_{n-1,s} > P_{n-1,t}$	$P_{n-1,s}$	sliding

If the lowest block with the actual mechanical parameters is stable, calculate the slope stability with these various $R_a < 1$, and FOS is the R_a that makes $P_0 \approx 0$. Similarly, if the lowest block with the actual mechanical parameters is unstable, the FOS is R_a ($R_a > 1$) which makes $P_0 \approx 0$.

The method can be easily carried out in spreadsheets such as Excel. The flow chart is shown in Figure 5, in which the number in front of the colon is the corresponding column in the calculation sheet, e.g., the column number in Table 3. The procedure will be described in more detail with a case study in the next section.

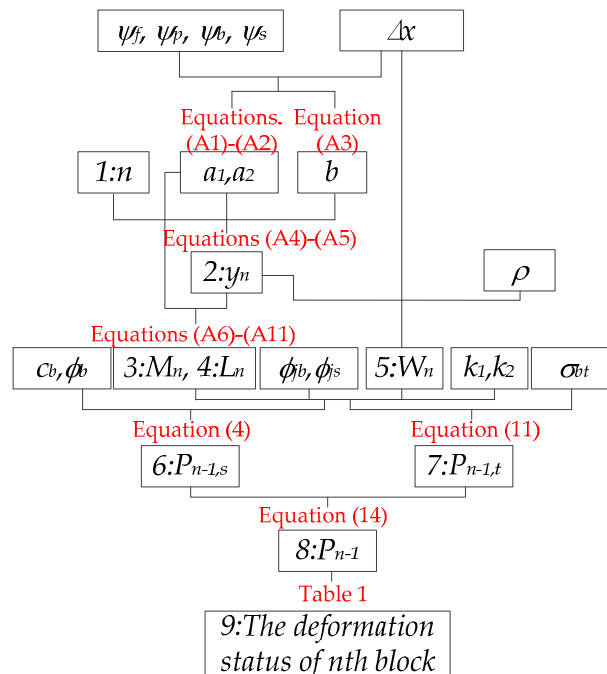


Figure 5. The flow chart to use the presented limit equilibrium method in sheet.

3. An Application Research on an Anti-Dip Rock Slope Model under Shake Table Test

A lot of research has been conducted on the dynamic response of rock slopes since the Wenchuan earthquake on 12 May 2008, e.g., the centrifuge test [24,25] and shake table test [26]. The latter one will be adopted to put forward a comparative study with the presented analytical solution.

The experiment was conducted using the shake table in the Institute of Engineering Mechanics China Earthquake Administration, which is 5 m × 5 m; maximum horizontal and vertical accelerations are 1.0 g and 0.8 g respectively. The size of the model box is 3.6 m (length) × 1.6 m (width) × 1.8 m (height). The height of the physical slope model is 1.6 m, the slope angle is 40°, and the anti-dip angle of the layer is 60°. The model is built from lots of small blocks of 20 cm (length) × 5 cm (width) × 4 cm (height) (Figure 6a). The density of the blocks is 2.51 g/cm³, the tensile strength σ_{bt} is 0.094 MPa, elastic modulus is 138.74 MPa, cohesion c_b is 0.711 MPa and internal friction angle θ_b is 36.2°. The friction angle of block side joints is 30°. The friction angle and cohesion of the block base joints are 30° and 0.35 MPa respectively [26]. All these parameters have an influence on the analytical results in the presented limit equilibrium method, so they are strictly following the real case to verify the practicability of the analytical method.

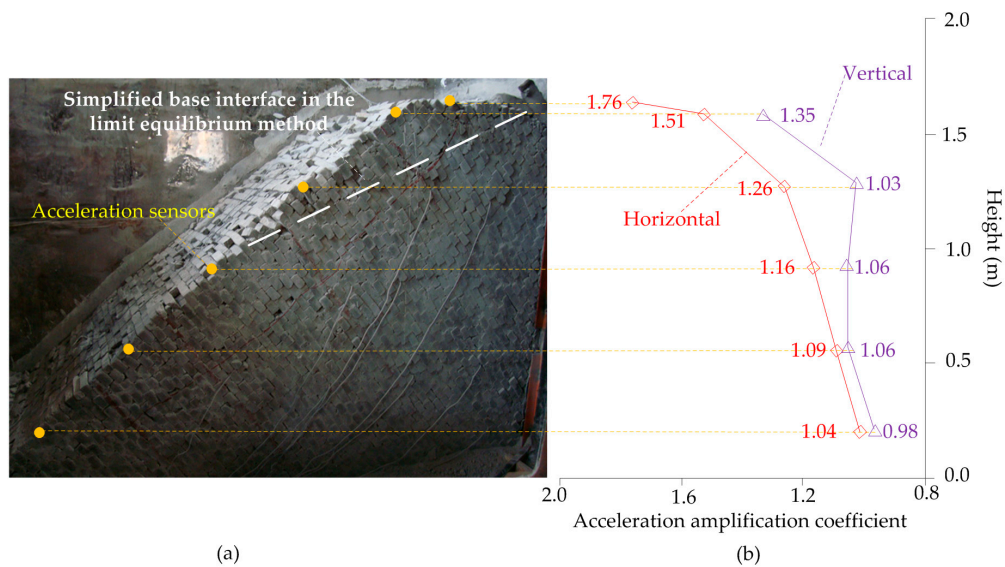


Figure 6. The large scale shake table test on anti-dip layered slope model: (a) the layout of acceleration sensors on the surface and the failure status of the slope model (modified based on [26]); (b) the acceleration amplification coefficients increase with slope height on the slope surface (data from [26]).

Sine waves with various frequency (5, 10, 15, 20 Hz), acceleration amplitude (0.1 g, 0.2 g, . . . , 0.8 g) and duration (10, 20, 30, 40 s) were input to study the dynamic response of the anti-dip slope. Rubber materials are used to eliminate the boundary effects. Acceleration sensors were laid out in horizontal and vertical lines to record the acceleration during the experiment in different positions, some of which are on the surface as shown in Figure 6a. A high speed camera was also used to record the progressive failure process.

The results of acceleration data show that the acceleration enlarges with elevation in the vertical direction and also enlarges near slope surface in the horizontal direction. This phenomenon has been observed by extensive researches (e.g., [27–29]) and known as amplification effects. In the shake table tests, it indicates that under low acceleration (<0.2 g), that the horizontal acceleration on the slope surface increased over 1.5 times above 3/4 slope height compared with that in the slope toe, while the vertical acceleration did not increase obviously in the same zone except at the top position (Figure 6b).

The progressive failure process with the increasing incident wave was recorded and described as follows [26]:

- (1) As the inputting acceleration (horizontal direction) increased to 0.3 g, some flexible toppling deformation initiated around the slope crest.
- (2) As the inputting accelerations (both horizontal and vertical direction) increased to 0.3 g, the number of toppling blocks increased a little and several blocks fell down.

- (3) As the inputting acceleration (horizontal direction) increased to 0.4 g, the toppling deformation was observed obviously and continued to develop noticeably around the slope crest.
- (4) As the inputting acceleration (horizontal direction) increased to 0.7 g, shear sliding deformation initiated in the slope, i.e., a curved-linear sliding surface was observed.
- (5) As the inputting acceleration (horizontal direction) increased to 0.8 g, the sliding surface propagated to nearly go through the crest area and some cracks parallel to the sliding surface were observed in the slope (Figure 6a).

An equilibrium slope model was built based on the shake table test as shown in Figure 7. The adjacent area around the slope crest is determined for the equilibrium model according to the observed deformation blocks in the physical experiment (the dashed white line in Figure 6a as the overall block base). There are 26 blocks in total and the geometric parameters are shown in Table 2. It should be mentioned that the J_c of the base interface is estimated approximately as 0.51 to be equivalent to the joint cohesion (about 0.51 times of block cohesion).

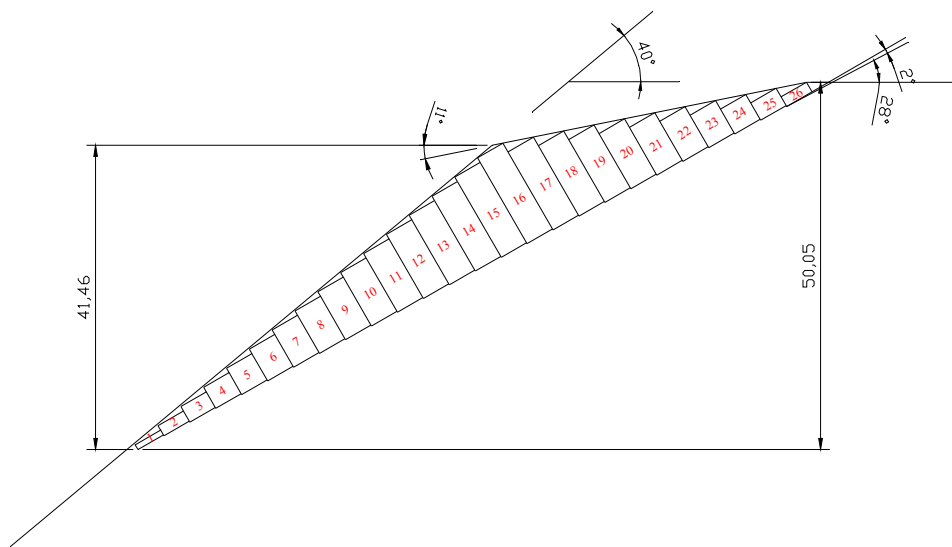


Figure 7. The limit equilibrium model for physical model on the shake table test

Table 2. The geometric parameters in the equilibrium slope model of shake table test (data based on [26]).

Parameter	Value	Parameter	Value
Δx (m)	0.04	ψ_f (°)	40
a_1 (m)	0.007	ψ_p (°)	30
a_2 (m)	0.0135	ψ_b (°)	28
b (m)	-0.0015	ψ_s (°)	11
J_c	0.51	-	-

The original model before the experiment would be analyzed firstly following the method described in the previous section (Figure 5) and also by the following steps:

Step 1. Calculating all the sizes needed using Equations (A1)–(A11); the results are shown in the 2nd to 4th columns in Table 3.

Step 2. Determining the physical parameters of blocks and joints, which were described above, and the block weight W_n which can be obtained from the 5th column in Table 3.

Step 3. Calculating $P_{n-1,s}$ and $P_{n-1,t}$ from the top block downwards on the basis of Equations (4) and (11) with $k_1 = 0$ and $k_2 = 0$ for the static state. The results are shown in the 6th and 7th columns in Table 3.

Step 4. Determining P_{n-1} of all the blocks according to $P_{n-1} = \max(P_{n-1,s}, P_{n-1,t}, 0)$, which are shown in the 8th column in Table 3.

Step 5. Determining the deformation status of all the blocks which is shown in the 9th column in Table 3.

Step 6. Estimating the stability of the slope according to the deformation status of the lowest block. It can be seen that the slope is stable under the static conditions.

Step 7. Determining the FOS of the slope. The results showed that the FOS of the slope is 4.6 under static conditions (Figure 8).

Table 3. The sheet from limit equilibrium analysis of slopes under static state.

1 <i>n</i>	2 <i>y_n</i> (cm)	3 <i>M_n</i> (cm)	4 <i>L_n</i> (cm)	5 <i>W_n</i> (N)	6 <i>P_{n,t}</i> (N)	7 <i>P_{n,s}</i> (N)	8 <i>P_n</i> (N)	9 MODE
26	1.5	0.2	1.5	15.1	0.0	0.0	0.0	
25	2.7	1.4	2.7	27.1	-390.2	-225.3	0.0	
24	3.9	2.6	3.9	39.2	-233.0	-226.6	0.0	
23	5.1	3.8	5.1	51.2	-165.9	-227.8	0.0	
22	6.3	5.0	6.3	63.3	-127.9	-229.1	0.0	
21	7.5	6.2	7.5	75.3	-102.7	-230.4	0.0	
20	8.7	7.4	8.7	87.3	-84.5	-231.6	0.0	
19	9.9	8.6	9.9	99.4	-70.3	-232.9	0.0	
18	11.1	9.8	11.1	111.4	-58.8	-234.2	0.0	
17	12.3	11.0	12.3	123.5	-49.1	-235.4	0.0	
16	13.5	12.2	12.8	135.5	-40.7	-236.7	0.0	
15	12.7	12.7	12.0	127.0	-35.1	-238.0	0.0	
14	11.8	11.8	11.1	118.5	-40.7	-237.1	0.0	
13	11.0	11.0	10.3	109.9	-46.8	-236.2	0.0	stable
12	10.1	10.1	9.4	101.4	-53.6	-235.3	0.0	
11	9.3	9.3	8.6	92.9	-61.3	-234.4	0.0	
10	8.4	8.4	7.7	84.3	-70.0	-233.5	0.0	
9	7.6	7.6	6.9	75.8	-80.1	-232.6	0.0	
8	6.7	6.7	6.0	67.3	-92.1	-231.7	0.0	
7	5.9	5.9	5.2	58.7	-106.9	-230.8	0.0	
6	5.0	5.0	4.3	50.2	-125.6	-229.9	0.0	
5	4.2	4.2	3.5	41.7	-150.7	-229.0	0.0	
4	3.3	3.3	2.6	33.1	-186.4	-228.1	0.0	
3	2.5	2.5	1.8	24.6	-242.4	-227.2	0.0	
2	1.6	1.6	0.9	16.1	-345.3	-226.3	0.0	
1	0.8	0.8	0.1	7.5	-603.4	-225.4	0.0	

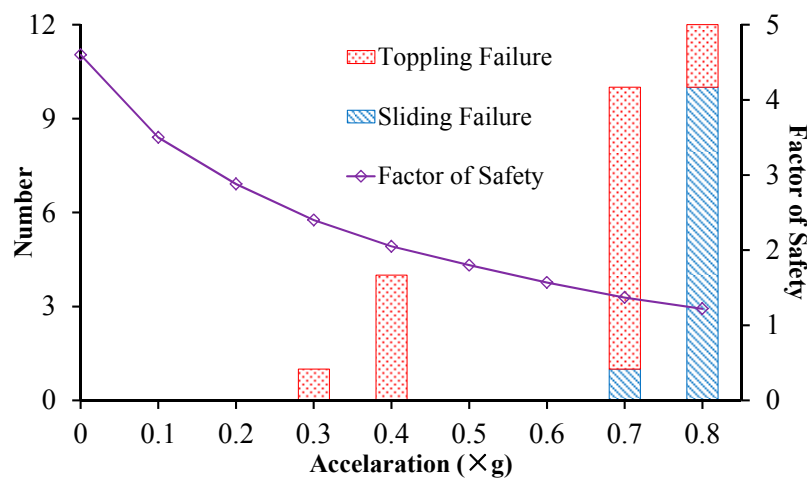


Figure 8. The deformation blocks and factor of safety (FOS) of the slope during the shake table test. (Accelerations in horizontal axis denote k_x with $k_y = 0$, and $k_x = k_y = 0.3$ g is excluded in this diagram).

Similarly, the limit equilibrium analysis for the slope under various dynamic loads is also carried out according to the steps described above. It should be noted that the acceleration amplification coefficient is also considered, i.e., 1.5 for the horizontal direction and 1 for the vertical direction. Furthermore, k_1 and k_2 are converted from k_x and k_y according to slope angle. Some critical sheets with horizontal accelerations of 0.3 g, 0.4 g, 0.7 g and 0.8 g are shown in Table 4. The corresponding FOS and the number of shearing and tensile blocks under varied accelerations are shown in Figure 8. The progressive deformation process derived by the presented method is detailed as follows.

- (1) The toppling deformation initiates at the dynamic loads of $k_x = 0.3$ g and $k_y = 0$, i.e., there is one toppling block near the slope crest (Table 4a and Figure 8).
- (2) As the accelerations (both horizontal and vertical direction) increased to 0.3 g, two toppling blocks were estimated (Table 4b).
- (3) As the acceleration (horizontal direction) increased to 0.4 g, four toppling blocks was estimated around the slope crest (Table 4c and Figure 8).
- (4) As the inputting acceleration (horizontal direction) increased to 0.7 g, shear sliding deformation initiated, i.e., 1 sliding block, and 9 toppling blocks were estimated in the slope (Table 4d and Figure 8).
- (5) As the inputting acceleration (horizontal direction) increased to 0.8g, the slope is nearly sheared through at $k_x = 0.8$ g and $k_y = 0$, which has 10 sliding blocks and 2 toppling blocks (Table 4e and Figure 8).

It seems that the proposed analytical solution can encompass nearly all of the deformation processes of the toppling slope model with five inputting accelerations during the shake table test depicted above. Besides, the FOS can be also reached as shown in Figure 8. It is indicated that the FOS decreases with the increase of dynamic loads, and reaches nearly 1 at $k_x = 0.8$ g and $k_y = 0$ (Figure 8), which indicates that the slope is close to the limit equilibrium state at this stage.

Table 4. The sheets from limit equilibrium analysis of slopes under seismic loads.

(a) $k_x = 0.3$ g, $k_y = 0$								
n	y_n (cm)	M_n (cm)	L_n (cm)	W_n (N)	$P_{n,i}$ (N)	$P_{n,s}$ (N)	P_n (N)	MODE
26	1.5	0.2	1.5	15.1	0.0	0.0	0.0	
25	2.7	1.4	2.7	27.1	-362.9	-212.3	0.0	
24	3.9	2.6	3.9	39.2	-210.8	-203.2	0.0	
23	5.1	3.8	5.1	51.2	-144.7	-194.1	0.0	
22	6.3	5.0	6.3	63.3	-106.2	-185.0	0.0	
21	7.5	6.2	7.5	75.3	-79.9	-175.8	0.0	Stable
20	8.7	7.4	8.7	87.3	-60.2	-166.7	0.0	
19	9.9	8.6	9.9	99.4	-44.3	-157.6	0.0	
18	11.1	9.8	11.1	111.4	-30.9	-148.5	0.0	
17	12.3	11.0	12.3	123.5	-19.3	-139.4	0.0	
16	13.5	12.2	12.8	135.5	-8.8	-130.3	0.0	
15	12.7	12.7	12.0	127.0	0.8	-121.1	0.8	Toppling
14	11.8	11.8	11.1	118.5	-5.6	-126.8	0.0	
13	11.0	11.0	10.3	109.9	-13.9	-134.1	0.0	
12	10.1	10.1	9.4	101.4	-22.0	-140.5	0.0	
11	9.3	9.3	8.6	92.9	-31.0	-147.0	0.0	
10	8.4	8.4	7.7	84.3	-41.0	-153.4	0.0	
9	7.6	7.6	6.9	75.8	-52.3	-159.9	0.0	
8	6.7	6.7	6.0	67.3	-65.4	-166.3	0.0	
7	5.9	5.9	5.2	58.7	-81.0	-172.8	0.0	Stable
6	5.0	5.0	4.3	50.2	-100.4	-179.3	0.0	
5	4.2	4.2	3.5	41.7	-125.8	-185.7	0.0	
4	3.3	3.3	2.6	33.1	-161.2	-192.2	0.0	
3	2.5	2.5	1.8	24.6	-215.8	-198.6	0.0	
2	1.6	1.6	0.9	16.1	-314.9	-205.1	0.0	
1	0.8	0.8	0.1	7.5	-562.4	-211.5	0.0	

Table 4. Cont.

(b) $k_x = 0.3 \text{ g}, k_y = 0.3 \text{ g}$									
n	y_n (cm)	M_n (cm)	L_n (cm)	W_n (N)	$P_{n,t}$ (N)	$P_{n,s}$ (N)	P_n (N)	MODE	
26	1.5	0.2	1.5	15.1	0.0	0.0	0.0	Stable	
25	2.7	1.4	2.7	27.1	-367.3	-212.8	0.0		
24	3.9	2.6	3.9	39.2	-214.6	-204.1	0.0		
23	5.1	3.8	5.1	51.2	-147.7	-195.3	0.0		
22	6.3	5.0	6.3	63.3	-108.3	-186.6	0.0		
21	7.5	6.2	7.5	75.3	-81.2	-177.9	0.0		
20	8.7	7.4	8.7	87.3	-60.6	-169.1	0.0		
19	9.9	8.6	9.9	99.4	-43.8	-160.4	0.0		
18	11.1	9.8	11.1	111.4	-29.6	-151.7	0.0		
17	12.3	11.0	12.3	123.5	-17.0	-142.9	0.0		
16	13.5	12.2	12.8	135.5	-5.7	-134.2	0.0		
15	12.7	12.7	12.0	127.0	5.0	-125.5	5.0		Toppling
14	11.8	11.8	11.1	118.5	1.5	-126.6	1.5		
13	11.0	11.0	10.3	109.9	-9.7	-136.3	0.0		
12	10.1	10.1	9.4	101.4	-19.8	-144.0	0.0		
11	9.3	9.3	8.6	92.9	-29.4	-150.2	0.0		
10	8.4	8.4	7.7	84.3	-40.0	-156.4	0.0		
9	7.6	7.6	6.9	75.8	-52.0	-162.6	0.0		
8	6.7	6.7	6.0	67.3	-65.8	-168.8	0.0		
7	5.9	5.9	5.2	58.7	-82.1	-174.9	0.0	Stable	
6	5.0	5.0	4.3	50.2	-102.3	-181.1	0.0		
5	4.2	4.2	3.5	41.7	-128.3	-187.3	0.0		
4	3.3	3.3	2.6	33.1	-164.5	-193.5	0.0		
3	2.5	2.5	1.8	24.6	-220.0	-199.7	0.0		
2	1.6	1.6	0.9	16.1	-320.3	-205.9	0.0		
1	0.8	0.8	0.1	7.5	-569.5	-212.1	0.0		
(c) $k_x = 0.4 \text{ g}, k_y = 0$									
n	y_n (cm)	M_n (cm)	L_n (cm)	W_n (N)	$P_{n,t}$ (N)	$P_{n,s}$ (N)	P_n (N)	MODE	
26	1.5	0.2	1.5	15.1	0.0	0.0	0.0	Stable	
25	2.7	1.4	2.7	27.1	-360.5	-208.0	0.0		
24	3.9	2.6	3.9	39.2	-207.5	-195.4	0.0		
23	5.1	3.8	5.1	51.2	-140.6	-182.8	0.0		
22	6.3	5.0	6.3	63.3	-101.3	-170.2	0.0		
21	7.5	6.2	7.5	75.3	-74.2	-157.7	0.0		
20	8.7	7.4	8.7	87.3	-53.7	-145.1	0.0		
19	9.9	8.6	9.9	99.4	-37.0	-132.5	0.0		
18	11.1	9.8	11.1	111.4	-22.9	-119.9	0.0		
17	12.3	11.0	12.3	123.5	-10.4	-107.4	0.0		
16	13.5	12.2	12.8	135.5	0.8	-94.8	0.8		Toppling
15	12.7	12.7	12.0	127.0	12.4	-81.4	12.4		
14	11.8	11.8	11.1	118.5	14.5	-78.7	14.5		
13	11.0	11.0	10.3	109.9	8.0	-85.5	8.0		
12	10.1	10.1	9.4	101.4	-6.3	-101.0	0.0		
11	9.3	9.3	8.6	92.9	-22.2	-117.8	0.0		
10	8.4	8.4	7.7	84.3	-32.7	-126.8	0.0		
9	7.6	7.6	6.9	75.8	-44.6	-135.7	0.0		
8	6.7	6.7	6.0	67.3	-58.2	-144.6	0.0		
7	5.9	5.9	5.2	58.7	-74.4	-153.5	0.0	Stable	
6	5.0	5.0	4.3	50.2	-94.3	-162.4	0.0		
5	4.2	4.2	3.5	41.7	-120.2	-171.3	0.0		
4	3.3	3.3	2.6	33.1	-156.1	-180.2	0.0		
3	2.5	2.5	1.8	24.6	-211.2	-189.1	0.0		
2	1.6	1.6	0.9	16.1	-310.7	-198.0	0.0		
1	0.8	0.8	0.1	7.5	-558.3	-206.9	0.0		

Table 4. Cont.

(d) $k_x = 0.7 \text{ g}, k_y = 0$									
n	y_n (cm)	M_n (cm)	L_n (cm)	W_n (N)	$P_{n,t}$ (N)	$P_{n,s}$ (N)	P_n (N)	MODE	
26	1.5	0.2	1.5	15.1	0.0	0.0	0.0	Stable	
25	2.7	1.4	2.7	27.1	-353.3	-195.0	0.0		
24	3.9	2.6	3.9	39.2	-197.7	-172.1	0.0		
23	5.1	3.8	5.1	51.2	-128.4	-149.1	0.0		
22	6.3	5.0	6.3	63.3	-86.6	-126.2	0.0		
21	7.5	6.2	7.5	75.3	-57.2	-103.3	0.0		
20	8.7	7.4	8.7	87.3	-34.3	-80.3	0.0		
19	9.9	8.6	9.9	99.4	-15.3	-57.4	0.0		
18	11.1	9.8	11.1	111.4	1.2	-34.4	1.2		
17	12.3	11.0	12.3	123.5	16.8	-10.2	16.8		Toppling
16	13.5	12.2	12.8	135.5	41.0	28.3	41.0	Sliding	
15	12.7	12.7	12.0	127.0	75.1	75.4	75.4		
14	11.8	11.8	11.1	118.5	98.4	93.6	98.4	Toppling	
13	11.0	11.0	10.3	109.9	106.7	100.3	106.7		
12	10.1	10.1	9.4	101.4	101.6	92.3	101.6		
11	9.3	9.3	8.6	92.9	84.6	71.0	84.6		
10	8.4	8.4	7.7	84.3	57.3	37.7	57.3		
9	7.6	7.6	6.9	75.8	21.3	-5.8	21.3		
8	6.7	6.7	6.0	67.3	-21.4	-58.0	0.0	Stable	
7	5.9	5.9	5.2	58.7	-54.5	-95.6	0.0		
6	5.0	5.0	4.3	50.2	-76.1	-111.9	0.0		
5	4.2	4.2	3.5	41.7	-103.5	-128.1	0.0		
4	3.3	3.3	2.6	33.1	-140.9	-144.4	0.0		
3	2.5	2.5	1.8	24.6	-197.4	-160.6	0.0		
2	1.6	1.6	0.9	16.1	-298.0	-176.9	0.0		
1	0.8	0.8	0.1	7.5	-546.0	-193.1	0.0		
(e) $k_x = 0.8 \text{ g}, k_y = 0$									
n	y_n (cm)	M_n (cm)	L_n (cm)	W_n (N)	$P_{n,t}$ (N)	$P_{n,s}$ (N)	P_n (N)		MODE
26	1.5	0.2	1.5	15.1	0.0	0.0	0.0	Stable	
25	2.7	1.4	2.7	27.1	-350.8	-190.7	0.0		
24	3.9	2.6	3.9	39.2	-194.4	-164.3	0.0		
23	5.1	3.8	5.1	51.2	-124.3	-137.8	0.0		
22	6.3	5.0	6.3	63.3	-81.7	-111.4	0.0		
21	7.5	6.2	7.5	75.3	-51.5	-85.0	0.0		
20	8.7	7.4	8.7	87.3	-27.8	-58.6	0.0		
19	9.9	8.6	9.9	99.4	-8.0	-32.1	0.0		
18	11.1	9.8	11.1	111.4	9.3	-5.7	9.3		
17	12.3	11.0	12.3	123.5	30.9	30.1	30.9		Toppling
16	13.5	12.2	12.8	135.5	60.3	78.1	78.1	Sliding	
15	12.7	12.7	12.0	127.0	113.7	151.7	151.7		
14	11.8	11.8	11.1	118.5	172.6	206.5	206.5		
13	11.0	11.0	10.3	109.9	205.6	242.6	242.6		
12	10.1	10.1	9.4	101.4	221.0	260.0	260.0		
11	9.3	9.3	8.6	92.9	219.0	258.7	258.7		
10	8.4	8.4	7.7	84.3	200.1	238.7	238.7		
9	7.6	7.6	6.9	75.8	164.8	200.0	200.0		
8	6.7	6.7	6.0	67.3	113.9	142.5	142.5		
7	5.9	5.9	5.2	58.7	48.8	66.4	66.4		
6	5.0	5.0	4.3	50.2	-28.3	-28.5	0.0	Stable	
5	4.2	4.2	3.5	41.7	-97.9	-113.6	0.0		
4	3.3	3.3	2.6	33.1	-135.8	-132.3	0.0		
3	2.5	2.5	1.8	24.6	-192.7	-151.0	0.0		
2	1.6	1.6	0.9	16.1	-293.8	-169.8	0.0		
1	0.8	0.8	0.1	7.5	-541.9	-188.5	0.0		

4. Discussion

A limit equilibrium analytical solution for the block toppling failure is presented and applied to an anti-dip rock slope model under shake table test. The theoretical results can capture the experimental observation well including the block deformation features and overall slope stability condition. In

the presented analytical analysis, some conditions are simplified, for example, the width of blocks is identical, the strength parameters are also identical for every block, and the failure base is a linear form. It is known that the real slopes in the field are sometimes much more complicated than the idealized slope mode. If so, the engineering geological generalization approach should be adopted to abstract the control factors and reach the simplified but representative engineering geological model. For the very complicated slopes such as those have unequal-sized layers and different variable strength parameters, numerical tools are more suitable [30].

The cohesion of layers or block base joints is not incorporated in the presented solution, because the cohesions of these discontinuities are effectively lost in most toppling slopes. If not, the presented solution should be modified a little to involve the cohesion of discontinuities, or an equivalent substitution can be used as we did in the case study. Besides, the discontinuity connectivity between adjacent blocks is considered as 1 to represent the bedding plane.

The acceleration amplification is another problem that should be discussed further. In the case study, the horizontal acceleration amplification coefficient increased with the slope height, over 1.5 near the crest. The vertical acceleration amplification coefficient does not increase as obviously as the horizontal one, i.e., around 1.0 except at the top of the slope where it is 1.35. The coefficient is assigned as 1.5 and 1.0 for the horizontal and vertical amplification respectively in the limit equilibrium analysis for simplicity. In the real slope, the coefficient may be much larger than 1.5 above the crest, so the tensile failure in these positions could always be observed at earliest stage during the failure process [31].

The presented solution is a form of deterministic analysis. If the inputting variables are not deterministic but probabilistic following certain distribution, the probability of failure can be calculated. This process is beyond the capacity of a sheet program but needs further study.

5. Conclusions

In this study, a limit equilibrium solution for block toppling failure is proposed. The seismic loads and connectivity of the block base joint are considered in the analytical solution. It is then applied into an anti-dip rock slope model under the shake table test. It confirms that the theoretical results can address most of the deformation features with the increasing incident wave during the shake table test, i.e., the modes, position of deformation blocks, and also the overall FOS. It can be concluded that the presented analytical solution is a universal method to estimate the block toppling deformation features and stability of anti-layered rock slopes with a non-persistent or persistent block base joint under static or seismic states.

Acknowledgments: The authors would like give great thanks to Ann Williams from New Zealand for her careful review and edit. This work is financially supported by the National Science Foundation of China under grants of No. 41672307, 41702345, China Postdoctoral Science Foundation under grant of Nos. 2017T100106, 2015M581167 and the National Key Research and Development Program of China under grant of 2017YFD0800501.

Author Contributions: Songfeng Guo and Shengwen Qi conceived and designed the experiments; Songfeng Guo, Shengwen Qi, and Guoxiang Yang performed the experiments; Songfeng Guo, Guoxiang Yang and Shishu Zhang analyzed the data; Songfeng Guo wrote the paper, Shengwen Qi and Charalampos Saroglou revised the paper.

Conflicts of Interest: The authors declare no conflict of interest.

Abbreviations

The following abbreviations are used in this manuscript:

H	Slope height
n	The number of the blocks (the block at the slope toe is numbered as 1 and $n = 1, 2, \dots$)
y_n	The height of n th block
Δx	The width of block
ψ_p	The dip of block base
ψ_d	The dip of the orthogonal planes forming the faces of the blocks
ψ_b	The overall dip of base plane
ψ_f	The slope angle under the crest
ψ_s	The slope angle above the crest
a_1	The height difference at the top of adjacent blocks under the slope crest
a_2	The height difference at the top of adjacent blocks above the slope crest
b	The height difference at the base of adjacent blocks
W_n	The weight of n th block
P_n	The normal force of $(n + 1)$ th block to n th block
Q_n	The shear force of $(n + 1)$ th block to n th block
P_{n-1}	The normal force of $(n - 1)$ th block to n th block
Q_{n-1}	The shear force of $(n - 1)$ th block to n th block
σ_{iM}	The maximum tensile stress induced by moment M_b
σ_{iR}	The compressive stress induced by R_n
R_n	The normal force of base to n th block
S_n	The shear force of base to n th block
M_n	The length from the point P_n to the base for the toppling block
L_n	The length from the point P_{n-1} to the base for the toppling block
M_b	The moment acting at the base of the toppling blocks
J_c	The joint connectivity rate of the block base
ξ	$1 - J_c$
k_1	Seismic acceleration component parallel to the block base
k_2	Seismic acceleration component orthogonal to the block base
k_x	Seismic acceleration component in horizontal direction
k_y	Seismic acceleration component in vertical direction
g	Gravitational acceleration
φ_{js}	Friction angle of block side
φ_{jb}	Friction angle of block base
φ_b	Internal friction angle of block
c_b	Cohesion of block
σ_{bt}	Tensile strength of block
ρ	Density of block

Appendix A

The approach to reach the geometric parameters (Goodman and Bray (1976)). The constants a_1 , a_2 and b in the slope geometry shown in Figure 2 can be given by:

$$a_1 = \Delta x \tan(\psi_f - \psi_p) \tag{A1}$$

$$a_2 = \Delta x \tan(\psi_p - \psi_s) \tag{A2}$$

$$b = \Delta x \tan(\psi_b - \psi_p) \tag{A3}$$

The slope model is divided into two parts, i.e., zone I that is the cut slope below the crest, zone II that has the natural topography above the crest. The blocks are numbered from the toe of the slope upwards, with the lowest block being 1. In this model, the height y_n of the n th block in zone I is:

$$y_n = n(a_1 - b) \tag{A4}$$

The height y_n of the n th block in zone II is:

$$y_n = y_{n-1} - a_2 - b \quad (\text{A5})$$

M_n and L_n are the distance from point of P_n and P_{n-1} to the block base respectively and can be reached by the following equations:

For the blocks in zone I,

$$M_n = y_n \quad (\text{A6})$$

$$L_n = y_n - a_1 \quad (\text{A7})$$

For the blocks in zone II,

$$M_n = y_n - a_2 \quad (\text{A8})$$

$$L_n = y_n \quad (\text{A9})$$

For the block in the crest,

$$M_n = y_n - a_2 \quad (\text{A10})$$

$$L_n = y_n - a_1 \quad (\text{A11})$$

References

- Chen, Z.; Wang, X.; Yang, J.; Jia, Z.; Wang, Y. *Rock Slope Stability Analysis—Theory, Methods and Programs*; China Water & Power Press: Beijing, China, 2005.
- Zhang, Z.; Liu, G.; Wu, S.; Tang, H.; Wang, T.; Li, G.; Liang, C. Rock slope deformation mechanism in the Cihaxia Hydropower Station, Northwest China. *Bull. Eng. Geol. Environ.* **2015**, *74*, 943–958. [[CrossRef](#)]
- Gu, D.; Huang, D. A complex rock topple-rock slide failure of an anticlinal rock slope in the Wu Gorge, Yangtze River, China. *Eng. Geol.* **2016**, *208*, 165–180. [[CrossRef](#)]
- Alejano, L.; Gómez-Márquez, I.; Martínez-Alegría, R. Analysis of a complex toppling-circular slope failure. *Eng. Geol.* **2010**, *114*, 93–104. [[CrossRef](#)]
- Wyllie, D.C. Toppling rock slope failures examples of analysis and stabilization. *Rock Mech.* **1980**, *13*, 89–98. [[CrossRef](#)]
- De Freitas, M.H.; Watters, R.J. Some field examples of toppling failure. *Geotechnique* **1973**, *23*, 495–513. [[CrossRef](#)]
- Huang, R.; Zhao, J.; Ju, N.; Li, G.; Lee, M.; Li, Y. Analysis of an anti-dip landslide triggered by the 2008 Wenchuan earthquake in China. *Nat. Hazards* **2013**, *68*, 1021–1039. [[CrossRef](#)]
- Goodman, R.E.; Bray, J.W. Toppling of rock slopes. In *Rock Engineering for Foundations & Slopes*; ASCE: Reston, VA, USA, 1976; pp. 201–234.
- Zanbak, C. Design charts for rock slopes susceptible to toppling. *J. Geotech. Eng.* **1983**, *109*, 1039–1062. [[CrossRef](#)]
- Bobet, A. Analytical solutions for toppling failure. *Int. J. Rock Mech. Min. Sci.* **1999**, *36*, 971–980. [[CrossRef](#)]
- Sagaseta, C.; Sanchez, J.; Canizal, J. A general analytical solution for the required anchor force in rock slopes with toppling failure. *Int. J. Rock Mech. Min. Sci.* **2001**, *38*, 421–435. [[CrossRef](#)]
- Liu, C.; Jaksá, M.; Meyers, A. Improved analytical solution for toppling stability analysis of rock slopes. *Int. J. Rock Mech. Min. Sci.* **2008**, *45*, 1361–1372. [[CrossRef](#)]
- Liu, C.; Chen, C. Analysis of toppling failure of rock slopes of rock slopes due to earthquakes. *Chin. J. Rock Mech. Eng.* **2010**, *29*, 3193–3198.
- Aydan, Ö.; Kawamoto, T. The stability of slopes and underground openings against flexural toppling and their stabilisation. *Rock Mech. Rock Eng.* **1992**, *25*, 143–165. [[CrossRef](#)]
- Adhikary, D.; Dyskin, A.; Jewell, R.; Stewart, D.P. A study of the mechanism of flexural toppling failure of rock slopes. *Rock Mech. Rock Eng.* **1997**, *30*, 75–93. [[CrossRef](#)]
- Majdi, A.; Amini, M. Analysis of geo-structural defects in flexural toppling failure. *Int. J. Rock Mech. Min. Sci.* **2011**, *48*, 175–186. [[CrossRef](#)]
- Yagoda-Biran, G.; Hatzor, Y. A new failure mode chart for toppling and sliding with consideration of earthquake inertia force. *Int. J. Rock Mech. Min. Sci.* **2013**, *64*, 122–131. [[CrossRef](#)]
- Zheng, Y.; Chen, C.; Zhu, X.; Liu, T.T.; Liu, X.M.; Song, Y.F.; Zhou, Y.C. Analysis of toppling failure of rock slopes subjected to seismic loads. *Rock Soil Mech.* **2014**, *35*, 1025–1032.

19. Maiorano, R.M.S.; Adinolfi, M.; Aversa, S. Rocking of slender rock blocks under seismic excitation. *Ital. Heotech. J.* **2015**, *49*, 87–99.
20. Zhang, Z.; Wang, T.; Wu, S.; Tang, H. Rock toppling failure mode influenced by local response to earthquakes. *Bull. Eng. Geol. Environ.* **2016**, *75*, 1361–1375. [[CrossRef](#)]
21. ROCSIENCE INC. *RocTopple Version 1.0-Toppling Analysis of Rock Slopes*; ROCSIENCE INC.: Toronto, ON, Canada, 2014. Available online: www.rocsience.com (accessed on 8 July 2017).
22. Wyllie, D.C.; Mah, C. *Rock Slope Engineering*; CRC Press: Boca Raton, FL, USA, 2004.
23. Pritchard, M.; Savigny, K. Numerical modelling of toppling. *Can. Geotech. J.* **1990**, *27*, 823–834. [[CrossRef](#)]
24. Alzo'ubi, A.; Martin, C.; Cruden, D. Influence of tensile strength on toppling failure in centrifuge tests. *Int. J. Rock Mech. Min. Sci.* **2010**, *47*, 974–982. [[CrossRef](#)]
25. Chen, Z.; Gong, W.; Ma, G.; Wang, J.; He, L.; Xing, Y.C.; Xing, J.Y. Comparisons between centrifuge and numerical modeling results for slope toppling failure. *Sci. China Technol. Sci.* **2015**, *58*, 1497–1508. [[CrossRef](#)]
26. Yang, G.; Ye, H.; Wu, F.; Qi, S.; Dong, J. Shaking table model test on dynamic response characteristics and failure mechanism of anti-dip layered rock slope. *Chin. J. Rock Mech. Eng.* **2012**, *31*, 2214–2221.
27. Qi, S.; Wu, F.Q.; Sun, J.Z. General regularity of dynamic responses of slopes under dynamic input. *Sci. China Ser. E* **2003**, *46*, 120–132. [[CrossRef](#)]
28. Bi, Z.W.; Zhang, M.; Jin, F.; Ding, D.X. Dynamic response of slopes under earthquakes. *Rock Soil Mech.* **2009**, *30*, 180–183.
29. Huang, R.; Li, G.; Ju, N. Shaking table test on strong earthquake response of stratified rock slopes. *Chin. J. Rock Mech. Eng.* **2013**, *32*, 865–876.
30. Lanaro, F.; Jing, L.; Stephansson, O.; Barla, G. DEM modelling of laboratory tests of block toppling. *Int. J. Rock Mech. Min. Sci.* **1997**, *34*, 209–218. [[CrossRef](#)]
31. Xu, Q.; Pei, X.; Huang, R. *Large-Scale Landslides Induced by Wenchuan Earthquake*; Science Press: Beijing, China, 2009. (In Chinese)



© 2017 by the authors. Licensee MDPI, Basel, Switzerland. This article is an open access article distributed under the terms and conditions of the Creative Commons Attribution (CC BY) license (<http://creativecommons.org/licenses/by/4.0/>).